Binding constants of membrane-anchored receptors and ligands depend strongly on the nanoscale roughness of membranes

Jinglei Hu[1], Reinhard Lipowsky, and Thomas R. Weikl[2]

Department of Theory and Bio-Systems, Max Planck Institute of Colloids and Interfaces, 14424 Potsdam, Germany

Cell adhesion and the adhesion of vesicles to the membranes of cells or organelles are pivotal for immune responses, tissue formation, and cell signaling. The adhesion processes depend sensitively on the binding constant of the membrane-anchored receptor and ligand proteins that mediate adhesion, but this constant is difficult to measure in experiments. We have investigated the binding of membrane-anchored receptor and ligand proteins with molecular dynamics simulations. We find that the binding constant of the anchored proteins strongly decreases with the membrane roughness caused by thermally excited membrane shape fluctuations on nanoscales. We present a theory that explains the roughness dependence of the binding constant for the anchored proteins from membrane confinement and that relates this constant to the binding constant of soluble proteins without membrane anchors. Because the binding constant of soluble proteins is readily accessible in experiments, our results provide a useful route to compute the binding constant of membrane-anchored receptor and ligand proteins.

protein binding | membrane adhesion | adhesion molecules | binding equilibrium and kinetics

A central problem in cell adhesion is to quantify the binding affinity of the membrane-anchored receptor and ligand proteins that cause adhesion (1–4). The distinction of "self" and "foreign" in cell-mediated immune responses, for example, depends on subtle affinity differences between receptor and ligand proteins anchored on the surfaces of apposing cells (5). The binding affinity of anchored receptor and ligand proteins, which are restricted to the two-dimensional (2D) membrane environment, is typically described by the binding equilibrium constant K_{2D} of the proteins. Because K_{2D} is difficult to measure in experiments, it is often estimated from the binding constant K_{3D} of soluble variants of the receptors and ligands that lack the membrane anchors and are free to diffuse in three dimensions (3D). Standard approaches are based on the relation $K_{2D} = K_{3D}/l_c$ suggested by Bell et al. (6), where l_c is a characteristic length that reflects the different units of area and volume for K_{2D} and K_{3D}, respectively. However, different methods to measure the binding equilibrium constant of membrane-anchored proteins have led to values of K_{2D} and associated values of l_c that differ by several orders of magnitude (7). In contrast to the standard approaches, the simulation data and theory presented here indicate that the relation between K_{2D} and K_{3D} involves three different length scales, and that the most important of these length scales is the membrane roughness resulting from shape fluctuations on nanoscales. Because the membrane roughness depends on the concentration of the receptor–ligand bonds that constrain the shape fluctuations, our results help to understand differences in K_{2D} values from different experiments.

In this article, we report simulations of biomembrane adhesion with a molecular model of lipids and proteins (Fig. 1A). We systematically vary the size of the membranes and the numbers of receptors and ligands and determine the binding constant K_{2D} and the on- and off-rate constants k_{on} and k_{off} of the membrane-anchored receptors and ligands for these different systems with high precision from thousands of binding and unbinding events

observed in our molecular dynamics simulations. Our largest apposing membranes are composed of 9,838 lipid molecules each and include 15 membrane-anchored receptors and ligands, respectively (Fig. 1C), whereas the smallest membranes contain 296 lipids and single receptor and ligand molecules. In addition, we determine the binding constant K_{3D} and the on- and off-rate constants of soluble variants of our receptors and ligands without membrane anchors.

We find that K_{2D} is not a constant, but depends strongly on the relative roughness $\xi_\perp$ of the apposing membranes. The relative membrane roughness is the local standard deviation (SD) of the membranes from their average separation due to thermally excited shape fluctuations. The relative roughness varies with the concentration of the bound receptor–ligand complexes because the complexes constrain membrane shape fluctuations. At the optimal average membrane separation for receptor–ligand binding, the binding constant K_{2D} is inversely proportional to the membrane roughness for roughnesses larger than about 0.5 nm and, thus, even for roughnesses that are significantly smaller than the membrane thickness.

To understand the roughness dependence of K_{2D} and the relation of K_{2D} to the binding equilibrium constant K_{3D} of soluble receptors and ligands without membrane anchors, we have developed a general theory in which the binding free energy of the receptor–ligand complexes is decomposed into enthalpic and entropic terms. We find that the roughness dependence of K_{2D} can be fully understood from the entropy loss of the membranes upon receptor–ligand binding. The theory is in good quantitative agreement with our simulation results and provides a unique route to calculate K_{2D} from experimental values for K_{3D}. In addition to the membrane roughness, our theory includes two characteristic lengths of the receptor–ligand complexes, which reflect variations in the overall extension and in the binding site of the complexes.

Results

Binding Constant K_{2D} of Membrane-Anchored Receptors and Ligands.
In our molecular dynamics simulations of biomembrane adhesion, the membranes are confined within a rectangular simulation box with periodic boundary conditions of size $L_x \times L_y \times L_z$. Whereas the box extension L_z in the direction perpendicular to the membranes has the same value in all simulations, the extensions $L_x = L_y$ are varied to simulate different membrane sizes (Fig. 1 B and C). Binding events of the receptor and ligand proteins in our simulations can be clearly identified from the distance between the binding sites of the proteins (Fig. 2). The binding equilibrium
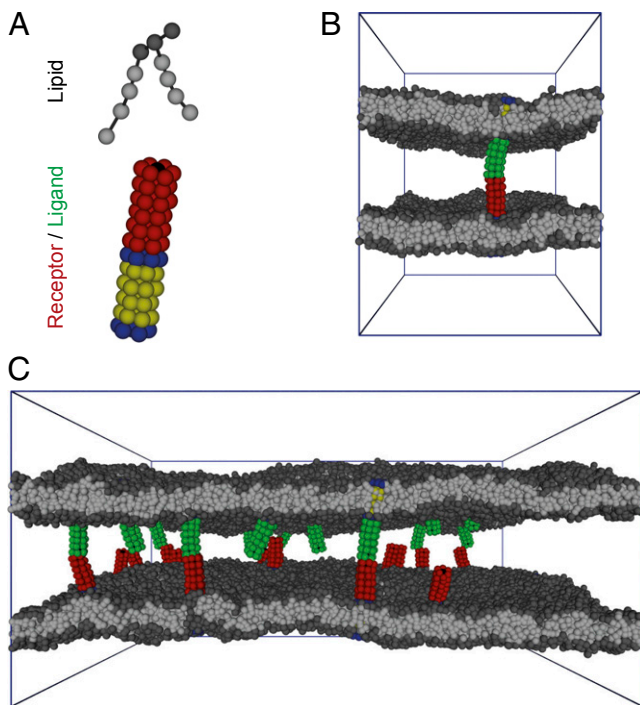

Fig. 1. (A) Coarse-grained structures of a lipid molecule and of a membrane-anchored receptor or ligand. The hydrophilic head group of a lipid molecule consists of three beads (dark gray), and the two hydrophobic chains are composed of four beads each (light gray) (8). The membrane-anchored receptors and ligands consist of 84 beads arranged in a cylindrical shape and have hydrophobic anchors that are embedded in the lipid bilayer and mimic the transmembrane segments of membrane proteins. The transmembrane anchor of a receptor or ligand molecule is composed of four layers of hydrophobic lipid-chain–like beads (yellow) in between two layers of lipid-head–like beads (blue). The interaction domain of the receptor and ligand molecules consists of six layers of hydrophilic beads (red), with an interaction bead or "binding site" located in the center of the top layer of beads (black). (B) Simulation snapshot of two apposing membranes bound together by a single anchored receptor and ligand molecule. For clarity, the interaction domain of the receptor is shown in red and the interaction domain of the ligand in green. Each membrane here has an area of 30 × 30 nm². (C) Simulation snapshot of two apposing membranes of area 80 × 80 nm² interacting via 15 anchored receptor and 15 ligand molecules. The water beads are not displayed in these snapshots.

constant K_{2D} of the anchored receptor and ligand proteins can then be calculated from the total dwell times in the bound and unbound states of the proteins observed in our simulations (*Model and Methods*).

The binding equilibrium constant and binding kinetics of membrane-anchored receptors and ligands depend on the distance between the two apposing membranes because receptor–ligand complexes cannot form if the two membranes are too far apart or too close. In Fig. 3, the binding constant K_{2D} of a single anchored receptor and a single anchored ligand molecule is shown as a function of the average membrane separation $\bar{l}$, which is kept constant in our simulations. In these simulations, the number of lipids is adjusted such that the membrane tension vanishes (8). For both membrane sizes $L_x \times L_y = 14 \times 14$ nm² and 30×30 nm², the binding constant K_{2D} is maximal at an average membrane separation close to the length of the receptor–ligand complexes. In the following, we will focus on the average membrane separation $\bar{l} = \bar{l}_0$ at which K_{2D} is maximal because maxima in K_{2D} correspond to minima of the free-energy difference between the bound and unbound state of the membranes (Eq. **5**). In a situation in which the membrane separation is not constrained, which is the typical

situation in experiments, the membranes thus will "choose" the "optimal" average membrane separation $\bar{l}_0$. Within numerical accuracy, the optimal average membrane separation obtained from our simulations does not depend on the membrane size.

In Fig. 3, the binding constants for the larger membrane area $L_x \times L_y = 30 \times 30$ nm² are significantly smaller than the binding constants for the membrane area $L_x \times L_y = 14 \times 14$ nm². These differences in the binding constants for different membrane sizes can be understood from the shape fluctuations of the membranes. A characteristic measure for the strength of the fluctuations is the relative roughness of the two membranes, which is the SD $\xi_\perp = \sqrt{\langle (l_i - \bar{l})^2 \rangle}$ of the local separation l_i of the membranes from the average separation $\bar{l} = \langle l_i \rangle$ where $\langle \ldots \rangle$ denotes the thermodynamic average. To calculate the roughness $\xi_\perp$, we divide the x-y plane of our simulation box, which is on average parallel to the membranes, into patches i of size 2×2 nm², and determine the local separation l_i of two apposing patches from the separation of the membrane midplanes. In Fig. 4, the binding constants K_{2D} from different membrane systems are shown as a function of the membrane roughness $\xi_\perp$ at the optimal average membrane separation $\bar{l}_0$. The binding constant K_{2D} of the membrane-anchored receptors and ligands clearly decreases with the relative roughness $\xi_\perp$ of the membranes. The data shown in Fig. 4 are from simulations of membrane systems that differ in membrane area, number of receptors and ligands, membrane tension, or membrane potential. The dark blue data points in Fig. 4 are from simulations with tensionless membranes and a single receptor and ligand. The different values for K_{2D} and $\xi_\perp$ in these simulations result from different membrane sizes. The arrows in Fig. 4 indicate the two points that correspond to the two maxima of Fig. 3 for the membrane sizes 14×14 nm² and 30×30 nm². The roughness for the membrane area 30×30 nm² is about a factor 2 larger than the roughness for the membrane area 14×14 nm², whereas the K_{2D} value at the optimal separation is about a factor 2 smaller for the membrane area 30×30 nm². The membrane roughness in our simulations depends on the size of the membranes because the periodic boundaries of the simulation box suppress membrane shape fluctuations with wavelength larger than $L_x/2\pi$, where $L_x = L_y$ is the linear membrane size. The purple data points in Fig. 4 are from simulations with eight receptors and eight ligands and a membrane area of $L_x \times L_y = 40 \times 40$ nm²,
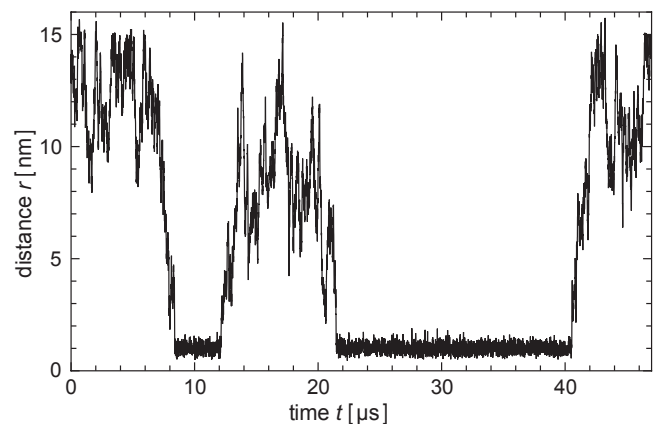
Fig. 2. Distance r between the binding sites of a single membrane-anchored receptor and ligand for a short time interval of a simulation with two apposing membranes of area 30 × 30 nm² as in Fig. 1B. Bound states of the receptor and ligand can be clearly identified from time segments in which the distance r between the centers of the binding sites exhibits small fluctuations around the value $r = 1$ nm at which the minimum of the binding potential is located. In this example, the receptor and ligand bind twice and unbind twice.

Fig. 3. Binding constant K_{2D} as a function of the average membrane separation $\bar{l}$ from simulations with membrane area $A = 14 \times 14$ nm^2 (upper) and 30×30 nm^2 (lower) and a single membrane-anchored receptor and ligand pair. The dashed lines are guides for the eye.

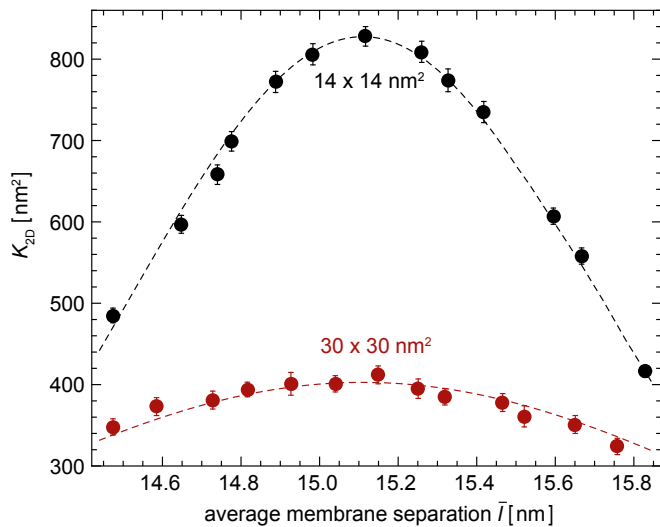and the brown data points from simulations with 15 receptors and 15 ligands and membrane area 80×80 nm^2. The different values for K_{2D} and $\xi_{\perp}$ in these simulations with tensionless membranes are for states with different numbers n of receptor–ligand bonds. These states exhibit different membrane roughnesses, as the receptor–ligand bonds constrain the membrane fluctuations (see *Model and Methods* for details). The three light blue data points are from simulations with positive (left point) or negative (two right points) membrane tension for the area 14×14 nm^2. Positive tension stretches the membranes and decreases the roughness, whereas negative tension compresses the membranes and increases the roughness. To extend the roughness range to smaller values, we have also performed simulations in which the membrane fluctuations are confined by membrane potentials (red points; see *SI Text* for details). In experiments, such a situation occurs for membranes bound to apposing surfaces as, for example, in the surface force apparatus (9, 10).

The fact that all data points of Fig. 4 collapse onto a single curve indicates that the relative membrane roughness $\xi_{\perp}$ determines K_{2D} irrespective of whether the size of $\xi_{\perp}$ is controlled by the membrane area, the concentration of the receptor–ligand complexes, the membrane tension, or confining membrane potentials. For roughnesses larger than about 0.5 nm, this curve can be well fitted by the inverse proportionality relation

$$K_{2D}/K_{3D} = (2.7 \pm 0.1)/\xi_{\perp} \qquad [1]$$

between the binding constant K_{2D} of the anchored receptors and ligands and the relative membrane roughness $\xi_{\perp}$ (see dashed line in Fig. 4). Here, K_{3D} is the binding constant of our soluble receptors and ligands without membrane anchors, which we have determined from simulations in water (see *SI Text* for details). The inverse proportionality between K_{2D} and the relative membrane roughness $\xi_{\perp}$ for sufficiently large roughnesses and the deviations from this proportionality for smaller roughness can be understood from a general theory for K_{2D} and K_{3D} derived in the next section.

A General Relation Between K_{2D} and K_{3D}. We first focus on K_{3D} and consider a single soluble receptor and a single soluble ligand in a volume V. The two molecules are bound with equilibrium probability P_b, and unbound with probability P_u. Detailed balance implies $P_u k_+ = P_b k_-$, where $k_+ = k_{on}/V$ and $k_- = k_{off}$ are the transition

rates between the bound and unbound state of the molecules. Because of $K_{3D} = k_{on}/k_{off}$, we have

$$K_{3D} = V \frac{P_b}{P_u} = V e^{-\Delta G_{3D}/k_B T}, \qquad [2]$$

where ΔG_{3D} is the binding free energy—that is, the free-energy difference between the bound and unbound state. We now consider the receptor and ligand as rigid rods with translational and rotational degrees of freedom. Following a standard approach in which the binding free energy is expanded around its minimum (11, 12), we obtain (see *SI Text* for details)

$$\Delta G_{3D} \simeq \Delta U - T\Delta S_{trans} - T\Delta S_{rot}$$
$$\simeq \Delta U - k_B T \ln\left[\frac{V_b}{V}\right] - k_B T \ln\left[\frac{\omega_b}{4\pi}\right] \qquad [3]$$

with the binding enthalpy ΔU and the loss ΔS_{trans} and ΔS_{rot} in translational and rotational entropy upon binding. Here, V_b is the translational phase space volume of the bound receptor relative to the ligand in the complex, and ω_b is the rotational phase space volume of the bound receptor relative to the ligand. In the
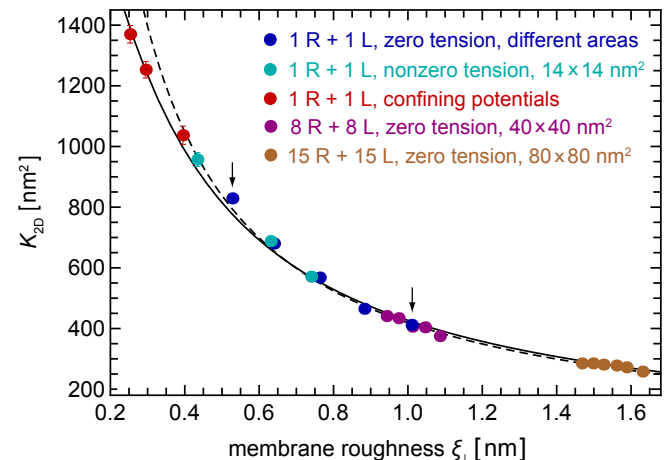
Fig. 4. Binding constant K_{2D} at the optimal membrane separation for receptor–ligand binding as a function of the relative roughness $\xi_{\perp}$ of the two apposing membranes caused by thermally excited membrane shape fluctuations. The dark blue data points are from simulations with single membrane-anchored receptor and ligand molecules and tensionless membranes of area $A = 14 \times 14$, 18×18, 22×22, 26×26, and 30×30 nm^2 (from left to right). The arrows indicate the two points that correspond to the maxima of Fig. 3 for the area 14×14 nm^2 (left arrow) and 30×30 nm^2 (right arrow). The light blue data points are from simulations with area 14×14 nm^2 and membrane tension 1.68 ± 0.01, -1.02 ± 0.02, and -1.50 ± 0.01 $k_B T$/nm^2 (from left to right). The red data points are from simulations with membrane area 14×14 nm^2 and confining potentials for head beads of the two distal monolayers of the membranes (see *SI Text* for details). The five purple data points are from simulations with eight receptor and eight ligand molecules and area 40×40 nm^2 of the two membranes, for the five binding reactions $n = 1 \rightleftharpoons 2 \rightleftharpoons 3 \rightleftharpoons 4 \rightleftharpoons 5 \rightleftharpoons 6$ (from right to left), where n is the number of formed receptor–ligand complexes. The six brown data points result from simulations with 15 receptors and 15 ligands and membrane area 80×80 nm^2 (Fig. 1C), for the six binding reactions $n = 2 \rightleftharpoons 3 \rightleftharpoons 4 \rightleftharpoons 5 \rightleftharpoons 6 \rightleftharpoons 7 \rightleftharpoons 8$ (from right to left). The dashed and full lines represent two fits to the data using the value $K_{3D} \simeq 157$ nm^3 for the binding constant of soluble receptors and ligands obtained from separate simulations. The dashed line is obtained from a least-square fit of the data points with roughness values larger than 0.5 nm to the functional form $K_{2D}/K_{3D} = C/\xi_{\perp}$, which leads to $C = 2.7 \pm 0.1$ as in Eq. **1**. The full line is obtained from a least-square fit of all data points to the functional form $K_{2D}/K_{3D} = C'/(\xi_{RL}^2 + \xi_{\perp}^2)^{1/2}$ given by Eq. **9**. This fit leads to $C' = 2.8 \pm 0.1$ and $\xi_{RL} = 0.2 \pm 0.1$ nm.

unbound state, the rod-like receptor and ligand rotate freely with rotational phase space volume 4π. Eqs. **2** and **3** lead to the general result

$$K_{3D} \simeq V_b \frac{\omega_b}{4\pi} e^{-\Delta U/k_B T} \qquad \text{[4]}$$

for the binding constant of soluble receptor and ligand molecules.

In analogy to the soluble molecules, we now consider a single pair of membrane-anchored receptor and ligand molecules in two apposing membranes of area A. The transition rates between the bound and unbound state of the molecules are $k_+ = k_{on}/A$ and $k_- = k_{off}$ (*Model and Methods*). The detailed balance condition $P_u k_+ = P_b k_-$ and the definition $K_{2D} = k_{on}/k_{off}$ then lead to

$$K_{2D} = A \frac{P_b}{P_u} = A e^{-\Delta G_{2D}/k_B T} \qquad \text{[5]}$$

with the free-energy difference ΔG_{2D} between the bound and unbound state. The free-energy difference can be decomposed as (see *SI Text* for details)

$$\begin{aligned}
\Delta G_{2D} &\simeq \Delta U - T\Delta S_{trans} - T\Delta S_{rot} - T\Delta S_{mem} \\
&\simeq \Delta U - k_B T \ln\left[\frac{A_b}{A}\right] - k_B T \ln\left[\frac{\omega_b \omega_{RL}}{\omega_R \omega_L}\right] \\
&\quad + \frac{k_B T}{2} \ln\left[1 + \frac{\xi_\perp^2}{\xi_{RL}^2}\right]
\end{aligned} \qquad \text{[6]}$$

with the translational and rotational entropy loss ΔS_{trans} and ΔS_{rot} of the receptor and ligand, and the entropy loss ΔS_{mem} of the membranes upon bond formation. Here, A_b is the translational phase space area of the bound receptor relative to the ligand in the two directions parallel to the membranes, ω_R and ω_L are the rotational phase space volumes of the unbound membrane-anchored receptor and ligand molecules relative to the membranes, and ω_{RL} is the rotational phase space volume of a bound receptor or bound ligand relative to the membranes. The entropy loss ΔS_{mem} of the membranes is obtained from exact results for a local harmonic constraint that restricts membrane shape fluctuations (13). This entropy loss depends on the relative roughness $\xi_\perp$ of the membranes and on a characteristic length ξ_{RL} that reflects intrinsic variations in the extension of the receptor–ligand complex in the direction perpendicular to the membranes, which result mainly from variations in the binding distance and anchoring angles of the molecules. Eqs. **5** and **6** lead to the general result

$$K_{2D} \simeq A_b \frac{\omega_b \omega_{RL}}{\omega_R \omega_L} \left[1 + \frac{\xi_\perp^2}{\xi_{RL}^2}\right]^{-\frac{1}{2}} e^{-\Delta U/k_B T} \qquad \text{[7]}$$

$$\simeq A_b \frac{\omega_b \omega_{RL}}{\omega_R \omega_L} \frac{\xi_{RL}}{\xi_\perp} e^{-\Delta U/k_B T} \quad \text{for} \quad \xi_\perp \gg \xi_{RL} \qquad \text{[8]}$$

for the binding constant of the membrane-anchored receptors and ligands.

Finally, from a combination of Eqs. **4**, **7**, and **8**, we obtain the general relation

$$\frac{K_{2D}}{K_{3D}} \simeq \frac{4\pi\omega_{RL}}{\omega_R \omega_L} \frac{\xi_{RL}}{\xi_b} \left(\xi_{RL}^2 + \xi_\perp^2\right)^{-\frac{1}{2}} \qquad \text{[9]}$$

$$\simeq \frac{4\pi\omega_{RL}}{\omega_R \omega_L} \frac{\xi_{RL}}{\xi_b \xi_\perp} \quad \text{for} \quad \xi_\perp \gg \xi_{RL} \qquad \text{[10]}$$

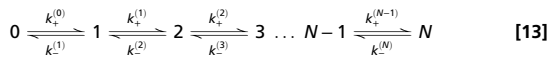between the binding equilibrium constant of the membrane-anchored molecules and the binding constant of their soluble counterparts without membrane anchors. We have assumed here that the binding interface of the membrane-anchored receptors and ligands is identical with the binding interface of their soluble counterparts (4), which implies that the binding enthalpy ΔU and the rational phase space volume ω_b of the bound receptor relative to the ligand are the same for both types of receptors and ligands. According to Eqs. **9** and **10**, the ratio K_{2D}/K_{3D} of the binding constants depends (*i*) on the membrane roughness $\xi_\perp$, (*ii*) on two characteristic lengths ξ_b and ξ_{RL} of the receptor–ligand complexes, and (*iii*) on the rotational phase space volumes ω_{RL}, ω_R, and ω_L of the bound and unbound membrane-anchored receptors and ligands. The characteristic length ξ_b of the receptor–ligand complexes is defined as $\xi_b = V_b/A_b$ and can be calculated from the SD of the distance between the binding sites in the direction parallel to the receptor–ligand complex, as V_b is the translational phase space volume of the bound complex and A_b the translational phase space area in the two directions perpendicular to the complex, and parallel to the membranes (see *SI Text* for details). We obtain the value $\xi_b \simeq 0.78$ nm for our receptor–ligand complexes. The characteristic length ξ_{RL} can be determined from a comparison with our simulation results for K_{2D} at the optimal membrane separation, which leads to the estimate $\xi_{RL} = 0.2 \pm 0.1$ nm (see full line in Fig. 4). The rotational phase space volumes ω_R, ω_L, and ω_{RL} can be calculated from the angular distributions of the receptors and ligands relative to the membranes. We obtain the values $\omega_R = \omega_L \simeq 0.75$ for our unbound receptors and ligands, and $\omega_{RL} \simeq 0.33$ for bound receptors or bound ligands. From these values and the values for the characteristic lengths ξ_b and ξ_{RL} of the receptor–ligand complexes given above, we obtain the estimate $(4\pi\omega_{RL}/\omega_R\omega_L)(\xi_{RL}/\xi_b) = 1.9 \pm 1.0$ for the numerical prefactor in Eqs. **9** and **10**, which is consistent with the values obtained from fits to our simulation results for K_{2D} at the optimal membrane separation (see Eq. **1** and caption of Fig. 4).

On- and Off-Rate Constants. Because K_{2D} can be expressed as the ratio of on- and off-rate constants k_{on} and k_{off} of the membrane-anchored receptors and ligands, an interesting question is whether the decrease of K_{2D} results from a decrease of k_{on} or an increase of k_{off} with the roughness, or both. We find that both k_{on} and k_{off} contribute to the roughness-dependence of K_{2D}, at least for the range of roughnesses accessible in our simulations (Fig. 5).

For the soluble receptors and ligands without membrane anchors, we obtain the off-rate $k_{off} = (4.0 \pm 0.1) \cdot 10^5$/s, which is about three to seven times larger than the off-rates obtained for the membrane-anchored receptor–ligand complexes. This finding is in agreement with experimental results for the binding of T-cell receptors to MHC-peptide ligands. The off-rates of soluble variants of these receptors and ligands without membrane anchors have been found to be slightly larger than the off-rates of the membrane-anchored receptors and ligands if the cytoskeleton of the cells is disrupted (14). In these experiments, the fluctuations of the cell membranes are governed by the membrane elasticity, as in our simulations. In experiments with intact cytoskeleton, the off-rates of membrane-anchored T-cell receptors and MHC-peptide ligands are larger than the off-rates of their soluble counterparts, presumably due to ATP-driven cytoskeletal forces acting on the membranes and receptor–ligand complexes (14–16).

Discussion and Conclusions

We have determined both the apparent binding constant K_{2D} of membrane-anchored receptors and ligands and the binding constant K_{3D} of soluble receptors and ligands with coarse-grained molecular dynamics simulations. In addition, we have developed a general theory for these binding constants that is in quantitative agreement with our simulation results. We find that K_{2D} is not a constant, but depends strongly on the membrane roughness $\xi_\perp$ from nanoscale shape fluctuations. In our general theory, the

Fig. 5. (A) On-rate constants k_{on} and (B) off-rates k_{off} of membrane-anchored receptors and ligands as a function of the relative membrane roughness $\xi_\perp$ from the same simulations as in Fig. 4.

roughness dependence of K_{2D} is traced back to the entropy loss of the membranes upon the formation of a receptor–ligand complex. Our general relations between K_{2D}, K_{3D}, and the relative membrane roughness $\xi_\perp$ hold for any membrane system in which the anchored proteins are rather rigid and do not oligomerize or aggregate. The optimal membrane separation of about 15 nm for our receptor–ligand complexes is close to the length of complexes of, for example, the T-cell receptor or the protein CD2 (1, 17). The concentrations of our anchored receptors and ligands between 2,000 and 5,000 molecules per μm^2 are somewhat larger than typical concentrations of these proteins (1, 14, 17). In our simulations, we also used relatively large on- and off-rates to ensure an efficient sampling of binding and unbinding events. Therefore, the kinetics of these events is strongly enhanced compared with protein binding events in experiments. It is important to note, however, that our main results for the ratio K_{2D}/K_{3D} of the binding constants are independent of the numerical values of the rate constants. These main results are (i) that K_{2D}/K_{3D} is inversely proportional to the membrane roughness $\xi_\perp$ for roughnesses large compared with the characteristic length ξ_{RL} of the anchored receptor–ligand complexes (Eqs. 1 and 10) and (ii) that the prefactor $(4\pi\omega_{RL}/\omega_R\omega_L)(\xi_{RL}/\xi_b)$ of this inverse proportionality depends only on the molecular geometry of the receptor–ligand complex (Eq. 10). To illustrate that K_{2D}/K_{3D} does not depend on the rate constants, we have performed additional simulations in which the binding energy of our receptors and ligands is increased by

25%. This increase in the binding energy increases both K_{2D} and K_{3D} by a factor 3.4 due to decreased off-rates, but does not change the ratio K_{2D}/K_{3D} (see *SI Text* for details).

The roughness-dependence of K_{2D} leads to unusual laws of mass action for the binding of membrane-anchored receptor and ligand molecules. Membrane adhesion zones are typically large compared with the average distance of about $1/\sqrt{[RL]}$ between neighboring receptor–ligand bonds. Because the bonds constrain the membrane shape fluctuations, the average bond distance is proportional to the relative roughness $\xi_\perp$ of the membranes, which leads to the relation (18)

$$\xi_\perp \propto 1/\sqrt{[RL]} \qquad [11]$$

between the roughness $\xi_\perp$ and the concentration $[RL]$ of receptor–ligand bonds. From Eq. 11 and the inverse proportionality of the binding constant $K_{2D} = [RL]/[R][L]$ and the relative roughness $\xi_\perp$ (Eq. 1), we obtain the quadratic relation

$$[RL] \propto [R]^2[L]^2 \qquad [12]$$

between the bond concentration $[RL]$ and the concentrations $[R]$ and $[L]$ of the unbound receptors and ligands, which corroborates previous results from an elasticity model of biomembrane adhesion (19). This quadratic law of mass action indicates a cooperative binding of membrane-anchored receptors and ligands.

Model and Methods

Simulations. Coarse-grained molecular dynamics simulations have been widely used to investigate the self-assembly (8, 20–22) and fusion (23–26) of membranes as well as the diffusion (27, 28) and aggregation (29) of membrane proteins. We have performed simulations with dissipative particle dynamics (30–32), a coarse-grained molecular dynamics technique that explicitly includes water. Our simulations of biomembrane adhesion include water beads, lipid molecules, and membrane receptors and ligands (Fig. 1). The lipid molecules consist of three hydrophilic head beads and two hydrophobic chains with four beads each, which are held together by harmonic potentials between adjacent beads and stiffened by bending potentials between three consecutive beads (8, 25, 26, 33). The membrane-anchored receptor and ligand molecules are composed of 84 beads that are arranged in a cylindrical shape of 12 hydrophobic or hydrophilic layers of seven beads each (Fig. 1A). Harmonic potentials between nearest and next-nearest neighbor beads lead to a rather stiff shape of the receptors and ligands. The specific binding of receptors and ligands is modeled via a distance- and angle-dependent attraction between two interaction beads that are located in the center of the top layers of beads (Fig. 1A). All other pairs of beads of the receptors, ligands, lipids, and water softly repel each other with a strength that depends on the bead types (see *SI Text* for details). In addition, we simulate the binding of soluble receptors and ligands in water. These soluble receptors and ligands lack the hydrophobic transmembrane anchor, but are otherwise identical with the membrane-anchored receptors and ligands.

Analysis of Binding Kinetics. Binding and unbinding events of receptor and ligand molecules in our simulations can be identified from the distance between the binding sites of these molecules (Fig. 2). To distinguish binding and unbinding events from distance fluctuations in the bound and unbound state, we use two distance thresholds to define these events. A binding event is defined to occur when the distance r between the binding sites of a receptor and ligand falls below the binding threshold $r_1 = 1$ nm. An unbinding event is defined to occur when the binding-site distance of a bound receptor–ligand pair exceeds the unbinding threshold $r_2 = 4$ nm, which is well beyond the range of fluctuations in the bound state. The values for K_{2D} and K_{3D} and the relative values of the on- and off-rate constants of the receptors and ligands obtained from our analysis do not depend on the precise values of these thresholds.

The binding and unbinding events divide our simulation trajectories into different states with different numbers of bound receptor–ligand complexes. In our simulations with a single receptor and ligand molecule, we have two states: the unbound state of the molecules and the bound state with a single receptor–ligand complex. In our simulations with N_R receptors and N_L ligands, we have $N + 1$ states where $N = \min(N_R, N_L)$ is the maximum number of bound complexes. Our simulation trajectories thus can be mapped to a Markov model:

$$0 \underset{k_-^{(1)}}{\overset{k_+^{(0)}}{\rightleftharpoons}} 1 \underset{k_-^{(2)}}{\overset{k_+^{(1)}}{\rightleftharpoons}} 2 \underset{k_-^{(3)}}{\overset{k_+^{(2)}}{\rightleftharpoons}} 3 \; \dots \; N-1 \underset{k_-^{(N)}}{\overset{k_+^{(N-1)}}{\rightleftharpoons}} N \qquad \text{[13]}$$

with transition rates $k_+^{(n)}$ and $k_-^{(n)}$ between the states that are related to the binding and unbinding rate constants $k_{\text{on}}^{(n)}$ and $k_{\text{off}}^{(n)}$ of the receptors and ligands. The binding rate of an individual unbound receptor in state n is proportional to the concentration $(N_L - n)/A$ of unbound ligands and proportional to the rate constant $k_{\text{on}}^{(n)}$ for the formation of a bond in state n, where A is the area of the membranes. Because we have $N_R - n$ unbound receptors, the rate for a transition from state n to state $n + 1$ is:

$$k_+^{(n)} = (1/A)(N_L - n)(N_R - n)k_{\text{on}}^{(n)} \qquad \text{[14]}$$

for $n < N$. The rate for a transition from state n to $n - 1$ is:

$$k_-^{(n)} = n k_{\text{off}}^{(n)} \qquad \text{[15]}$$

for $n > 0$ because there are n bonds that may each break with rate $k_{\text{off}}^{(n)}$. The binding constant is defined as:

$$K_{2D}^{(n)} = \frac{k_{\text{on}}^{(n-1)}}{k_{\text{off}}^{(n)}}. \qquad \text{[16]}$$

The on- and off-rate constants can be determined from the observed numbers of transitions between the states and from the overall dwell times in the states. The binding and unbinding events divide the simulation trajectories into time windows i of length t_i in state n_i, which are followed by a transition into state $n_i + s_i$, where s_i is either 1 or -1. The probability for staying for a dwell time t_i in state n_i is $P_{n_i}(t_i) = \exp[-(k_+^{(n_i)} + k_-^{(n_i)})t]$ with $k_-^{(0)} = k_+^{(N)} = 0$ (*SI Text*). The probability of time window i with its observed transition then is $p_i \propto P_{n_i}(t_i)k_+^{(n_i)}$ for $s_i = 1$ and $p_i \propto P_{n_i}(t_i)k_-^{(n_i)}$ for $s_i = -1$. The likelihood function is the probability for the whole trajectory—that is:

$$L = \prod_i p_i = \prod_{n=0}^{N} \left[k_+^{(n)}\right]^{N_n^+} \left[k_-^{(n)}\right]^{N_n^-} e^{-[k_+^{(n)} + k_-^{(n)}]T_n}, \qquad \text{[17]}$$

where N_n^+ is the total number of transitions from n to $n + 1$, N_n^- the total number of transitions from n to $n - 1$, and T_n the total dwell time in state n.

Maximizing L with respect to the binding and unbinding rate constants $k_{\text{on}}^{(n)}$ and $k_{\text{off}}^{(n)}$ of Eqs. **14** and **15** leads to the maximum likelihood estimators for the rate constants:

$$k_{\text{on}}^{(n)} = \frac{N_n^+ A}{(N_R - n)(N_L - n)T_n} \quad \text{and} \quad k_{\text{off}}^{(n)} = \frac{N_n^-}{nT_n}. \qquad \text{[18]}$$

Our estimator for the binding constant defined in Eq. **16** then is:

$$K_{2D}^{(n)} = \frac{nAT_n}{(N_R - n + 1)(N_L - n + 1)T_{n-1}} \qquad \text{[19]}$$

because the transition numbers N_{n-1}^+ and N_n^- are identical in equilibrium. For our simulations with a single receptor and a single ligand, the maximum-likelihood estimators for the on- and off-rate constants thus are $k_{\text{on}}^{(0)} = N_0^+ A/T_0$ and $k_{\text{off}}^{(1)} = N_1^-/T_1$, and the estimator for the binding constant is $K_{2D}^{(1)} = AT_1/T_0$. For large numbers N_R and N_L of receptors and ligands and states with $n \simeq \bar{n}$ receptor–ligand bonds where $\bar{n}$ is the average number of bonds, Eq. **19** is equivalent to $K_{2D} = [RL]/[R][L]$ with $[RL] = \bar{n}/A$, $[R] = (N_R - \bar{n})/A$, and $[L] = (N_L - \bar{n})/A$ as we then have $T_n \simeq T_{n-1}$ and $N_R - n + 1 \simeq N_R - n$.

1. Dustin ML, Ferguson LM, Chan PY, Springer TA, Golan DE (1996) Visualization of CD2 interaction with LFA-3 and determination of the two-dimensional dissociation constant for adhesion receptors in a contact area. *J Cell Biol* 132(3):465–474.
2. Zhu D-M, Dustin ML, Cairo CW, Golan DE (2007) Analysis of two-dimensional dissociation constant of laterally mobile cell adhesion molecules. *Biophys J* 92(3):1022–1034.
3. Leckband D, Sivasankar S (2012) Cadherin recognition and adhesion. *Curr Opin Cell Biol* 24(5):620–627.
4. Wu Y, Vendome J, Shapiro L, Ben-Shaul A, Honig B (2011) Transforming binding affinities from three dimensions to two with application to cadherin clustering. *Nature* 475(7357):510–513.
5. Alberts B, et al. (2008) *Molecular Biology of the Cell* (Garland Science, New York).
6. Bell GI, Dembo M, Bongrand P (1984) Cell adhesion. Competition between nonspecific repulsion and specific bonding. *Biophys J* 45(6):1051–1064.
7. Dustin ML, Bromley SK, Davis MM, Zhu C (2001) Identification of self through two-dimensional chemistry and synapses. *Annu Rev Cell Dev Biol* 17:133–157.
8. Goetz R, Lipowsky R (1998) Computer simulations of bilayer membranes: Self-assembly and interfacial tension. *J Chem Phys* 108(17):7397–7409.
9. Israelachvili JN (1992) *Intermolecular and surface forces* (Academic Press, Waltham, MA), 2nd Ed.
10. Bayas MV, Kearney A, Avramovic A, van der Merwe PA, Leckband DE (2007) Impact of salt bridges on the equilibrium binding and adhesion of human CD2 and CD58. *J Biol Chem* 282(8):5589–5596.
11. Luo H, Sharp K (2002) On the calculation of absolute macromolecular binding free energies. *Proc Natl Acad Sci USA* 99(16):10399–10404.
12. Woo H-J, Roux B (2005) Calculation of absolute protein-ligand binding free energy from computer simulations. *Proc Natl Acad Sci USA* 102(19):6825–6830.
13. Netz RR (1997) Inclusions in fluctuating membranes: Exact results. *J Phys I* 7(7):833–852.
14. Huppa JB, et al. (2010) TCR-peptide-MHC interactions in situ show accelerated kinetics and increased affinity. *Nature* 463(7283):963–967.
15. Huang J, et al. (2010) The kinetics of two-dimensional TCR and pMHC interactions determine T-cell responsiveness. *Nature* 464(7290):932–936.
16. Axmann M, Huppa JB, Davis MM, Schütz GJ (2012) Determination of interaction kinetics between the T cell receptor and peptide-loaded MHC class II via single-molecule diffusion measurements. *Biophys J* 103(2):L17–L19.
17. Grakoui A, et al. (1999) The immunological synapse: A molecular machine controlling T cell activation. *Science* 285(5425):221–227.
18. Krobath H, Schütz GJ, Lipowsky R, Weikl TR (2007) Lateral diffusion of receptor-ligand bonds in membrane adhesion zones: Effect of thermal membrane roughness. *Europhys Lett* 78(3):38003.
19. Krobath H, Rozycki B, Lipowsky R, Weikl TR (2009) Binding cooperativity of membrane adhesion receptors. *Soft Matter* 5(17):3354–3361.
20. Shelley JC, Shelley MY, Reeder RC, Bandyopadhyay S, Klein ML (2001) A coarse grain model for phospholipid simulations. *J Phys Chem B* 105(19):4464–4470.
21. Marrink SJ, de Vries AH, Mark AE (2004) Coarse grained model for semiquantitative lipid simulations. *J Phys Chem B* 108(2):750–760.
22. Shih AY, Arkhipov A, Freddolino PL, Schulten K (2006) Coarse grained protein-lipid model with application to lipoprotein particles. *J Phys Chem B* 110(8):3674–3684.
23. Marrink SJ, Mark AE (2003) The mechanism of vesicle fusion as revealed by molecular dynamics simulations. *J Am Chem Soc* 125(37):11144–11145.
24. Shillcock JC, Lipowsky R (2005) Tension-induced fusion of bilayer membranes and vesicles. *Nat Mater* 4(3):225–228.
25. Grafmüller A, Shillcock J, Lipowsky R (2007) Pathway of membrane fusion with two tension-dependent energy barriers. *Phys Rev Lett* 98(21):218101.
26. Grafmüller A, Shillcock J, Lipowsky R (2009) The fusion of membranes and vesicles: Pathway and energy barriers from dissipative particle dynamics. *Biophys J* 96(7):2658–2675.
27. Gambin Y, et al. (2006) Lateral mobility of proteins in liquid membranes revisited. *Proc Natl Acad Sci USA* 103(7):2098–2102.
28. Guigas G, Weiss M (2006) Size-dependent diffusion of membrane inclusions. *Biophys J* 91(7):2393–2398.
29. Reynwar BJ, et al. (2007) Aggregation and vesiculation of membrane proteins by curvature-mediated interactions. *Nature* 447(7143):461–464.
30. Hoogerbrugge PJ, Koelman JMVA (1992) Simulating microscopic hydrodynamic phenomena with dissipative particle dynamics. *Europhys Lett* 19(3):155–160.
31. Espanol P, Warren P (1995) Statistical mechanics of dissipative particle dynamics. *Europhys Lett* 30(4):191–196.
32. Groot RD, Warren PB (1997) Dissipative particle dynamics: Bridging the gap between atomistic and mesoscopic simulation. *J Chem Phys* 107(11):4423–4435.
33. Shillcock JC, Lipowsky R (2002) Equilibrium structure and lateral stress distribution of amphiphilic bilayers from dissipative particle dynamics simulations. *J Chem Phys* 117(10):5048–5061.

Supporting Information

Hu et al. 10.1073/pnas.1305766110

SI Text

Model and Simulations

Simulation Method. We have performed dissipative particle dynamics (DPD) simulations (1–3). DPD is a coarse-grained molecular dynamics technique that explicitly includes water (3). The DPD particles, or "beads," represent either a number of identical molecules or several molecular groups, rather than single atoms. The internal degrees of freedom of these molecules or molecular groups are reflected by dissipative forces and random forces, and the chemical nature of the molecules and molecular groups—for example, their hydrophobicity and hydrophilicity—is taken into account by conservative forces. Because all forces conserve momentum, DPD reproduces the correct hydrodynamics (3).

The DPD force that a bead j exerts on a bead i is the sum of three pairwise-additive forces: (*i*) the conservative force $\mathbf{F}_{ij}^C$, which results from bonded and nonbonded interactions of the beads; (*ii*) the dissipative or viscous friction force $\mathbf{F}_{ij}^D$; and (*iii*) the random force $\mathbf{F}_{ij}^R$. The dissipative force $\mathbf{F}_{ij}^D$ is related to the relative velocity $\mathbf{v}_{ij} = \mathbf{v}_i - \mathbf{v}_j$ of the beads via

$$\mathbf{F}_{ij}^D = \begin{cases} -\gamma_{ij}(1 - r_{ij}/r_0)^2 (\hat{\mathbf{r}}_{ij} \cdot \mathbf{v}_{ij})\hat{\mathbf{r}}_{ij}, & r_{ij} < r_0 \\ 0, & r_{ij} \ge r_0 \end{cases} \quad \text{[S1]}$$

with a friction coefficient $\gamma_{ij} = \gamma_{ji}$ that depends on the bead type. Here, $r_{ij} = |\mathbf{r}_i - \mathbf{r}_j|$ denotes the distance between the beads, $\hat{\mathbf{r}}_{ij} = (\mathbf{r}_i - \mathbf{r}_j)/r_{ij}$ is the unit vector pointing from bead j to bead i, and r_0 is the diameter of the beads. The random force $\mathbf{F}_{ij}^R$ representing thermal noise has the form:

$$\mathbf{F}_{ij}^R = \begin{cases} \sqrt{2\gamma_{ij}k_B T}(1 - r_{ij}/r_0)\zeta_{ij}\hat{\mathbf{r}}_{ij}, & r_{ij} < r_0 \\ 0, & r_{ij} \ge r_0 \end{cases}. \quad \text{[S2]}$$

Here, k_B is Boltzmann's constant, T is the temperature, and the Gaussian white-noise ζ_{ij} satisfies the stochastic properties $\langle \zeta_{ij}(t) \rangle = 0$ and $\langle \zeta_{ij}(t)\zeta_{i'j'}(t') \rangle = (\delta_{ii'}\delta_{jj'} + \delta_{ij'}\delta_{ji'})\delta(t - t')$ as well as the symmetry property $\zeta_{ij}(t) = \zeta_{ji}(t)$.

Bonded Interactions. Our coarse-grained model includes water, lipid molecules, and receptor and ligand molecules. Water molecules (W) are represented by single beads. A lipid molecule consists of three hydrophilic head beads (H) and two hydrophobic chains (C) with four beads each (4–7) (Fig. 1*A*). Adjacent beads are connected via harmonic potentials

$$V_{\text{bond}}(r) = \frac{1}{2}k_r(r - l_0)^2, \quad \text{[S3]}$$

with bond strength $k_r = 128 \, k_B T/r_0^2$ and preferred bond length $l_0 = 0.5 \, r_0$ (5). Here, r is the distance between the two beads. The two hydrophobic chains of the lipid molecules are stiffened by the bending potential (4)

$$V_{\text{bend}}(\phi) = k_\phi[1 - \cos(\phi - \phi_0)] \quad \text{[S4]}$$

that acts between two consecutive bonds along each chain. The bending constant is $k_\phi = 15 \, k_B T$, and the bond angle ϕ attains the preferred value $\phi_0 = 0$ for collinear bonds (6, 7).

The anchored receptor and ligand molecules consist of a transmembrane segment and an interaction segment (Fig. 1*A*). The transmembrane segment is composed of four layers of lipid-chain–like beads (T_C), which are shown in yellow in Fig. 1*A*, in between two layers of lipid-head–like beads (T_H) shown in blue. The interaction segment consists of six layers of a hydrophilic bead type I. Each pair of nearest neighboring beads of a receptor or ligand is connected by a harmonic potential with bond strength $k_r = 128 \, k_B T/r_0^2$ and bond length $l_0 = 0.875 \, r_0$. This bond length corresponds to the average distance of neighboring water beads in our simulations with bead density $\rho = 3 \, r_0^{-3}$. Each pair of next-nearest neighboring beads in two adjacent layers of a receptor or ligand is connected by a harmonic potential with bond strength $k_r = 128 \, k_B T/r_0^2$ and bond length $l_0 = \sqrt{2} \times 0.875 \, r_0$.

Nonbonded Interactions. In addition to the forces resulting from the bonded interactions specified above, all pairs of DPD beads—except for the interaction beads of a receptor and a ligand—exhibit the soft repulsive forces

$$\mathbf{F}_{ij}^C = \begin{cases} a_{ij}(1 - r_{ij}/r_0)\hat{\mathbf{r}}_{ij} & r_{ij} < r_0 \\ 0, & r_{ij} \ge r_0 \end{cases} \quad \text{[S5]}$$

with a repulsion strength a_{ij} that depends on the types of the two beads i and j (Table S1). The different repulsion strengths reflect the chemical nature of the beads—that is, their hydrophobicity or hydrophilicity. To avoid a clustering of receptors and ligands, the repulsion strength between the beads of two different receptors or two different ligands adopts the value $a_{ij} = 75 \, k_B T/r_0$, which is larger than the repulsion strength $a_{ij} = 25 \, k_B T/r_0$ between two beads of the same receptor, same ligand, or a receptor and a ligand. The friction coefficient γ_{ij} of the dissipative forces given by Eq. **S1** between two beads is affected by their repulsion strength as (5):

$$\gamma_{ij} = \begin{cases} 4.5, & a_{ij} < 35 \\ 9.0, & 35 \le a_{ij} < 75 \\ 20.0, & a_{ij} \ge 75 \end{cases}. \quad \text{[S6]}$$

The friction coefficient is given here in units of $\sqrt{m_0 k_B T/r_0^2}$, where m_0 is the bead mass.

The specific binding of a receptor and a ligand molecule is modeled via the binding potential

$$V_{\text{bind}}(r, \theta) = v_{\text{bind}}(r)e^{-k_\theta(\theta - \theta_0)^2}, \quad \text{[S7]}$$

which depends both on the distance r between the interaction beads of the receptors and ligands and on the angle θ between the two molecules. The interaction beads are located in the center of the top layer of the receptors' and ligands' interaction regions and are indicated in black in Fig. 1*A*. The angle θ between a receptor and a ligand molecule is defined as the angle between the two bonds that connect the interaction beads of the molecules to the central beads of the adjacent bead layers. The distance-dependent term $v_{\text{bind}}(r)$ of the specific interaction is

$$v_{\text{bind}}(r) = \begin{cases} \frac{1}{2}r_0(a_{\text{II}}(1 - r/r_0)^2 - F_m), & r < r_0 \\ F_m r_0((1 - r/r_0)^2 - \frac{1}{2}), & r_0 \le r < \frac{3}{2}r_0 \\ -F_m r_0(2 - r/r_0)^2, & \frac{3}{2}r_0 \le r < 2r_0 \\ 0, & r \ge 2r_0 \end{cases} \quad \text{[S8]}$$

with the DPD repulsion strength $a_{II} = 25\, k_B T / r_0$ and the attraction strength $F_m = 16\, k_B T / r_0$ (Fig. S1A). Differentiating $v_{bind}(r)$ with respect to r leads to the radial force component

$$F_{bind}(r) = \begin{cases} a_{II}(1 - r/r_0), & r < r_0 \\ 2F_m(1 - r/r_0), & r_0 \leq r < \frac{3}{2}r_0 \\ 2F_m(r/r_0 - 2), & \frac{3}{2}r_0 \leq r < 2r_0 \\ 0, & r \geq 2r_0 \end{cases}, \qquad \textbf{[S9]}$$

which includes a soft repulsion for $r < r_0$ and an attraction for $r_0 \leq r < 2\, r_0$ (Fig. S1B). The parameter k_θ in the binding potential S7 determines the width of the binding angle distribution and is chosen to be $k_\theta = 10\, \text{rad}^{-2}$ here. The angle θ between the two molecules adopts the preferred value $\theta_0 = 0$ if the two molecules are facing each other. The binding potential attains its minimum value of $-\frac{1}{2}F_m\, r_0 = -8\, k_B T$ at $r = r_0$ and $\theta = \theta_0$. For this intermediate binding energy of the receptors and ligands, both stable bonds and a large number of binding and unbinding events can be observed in our simulations.

DPD Simulations. In each simulation, the number density of DPD beads in the rectangular simulation box of size $V = L_x \times L_y \times L_z$ is set to $\rho = 3\, r_0^{-3}$. The total number of beads in each simulation system thus is ρV. The Newton's equations of motion are numerically integrated with a time step $t_0 = 0.03\sqrt{m_0 r_0^2 / k_B T}$ using the velocity-Verlet algorithm as in ref. 3. For this time step, the average temperature of the beads deviates from the expected value by at most 2%. Our optimized DPD code is parallelized to achieve a speedup of about a factor 6 by using eight central processing unit (CPU) cores, which enables us to simulate up to tens of thousands of binding and unbinding events to determine the binding constants with high accuracy. A relaxation run of $2 - 5 \cdot 10^6\, t_0$ is performed for thermal equilibrium in each system before statistical sampling.

Physical length and time scales for the bead diameter r_0 and for the step width t_0 of our simulations can be obtained from a comparison with experimental data for dimyristoyl-phosphatidylcholine (DMPC) bilayers (6, 7). Our model lipids correspond to the phospholipid DMPC as each C bead of the lipid tails can be seen to represent 3.5 CH_2 groups (4, 6), which leads to a total tail length of 14 CH_2 groups as for DMPC. To obtain a physical length scale for the bead diameter r_0, we compare experimental data for the thickness of fluid DMPC bilayers or, more precisely, for the vertical distance d_{HH} between the head groups of the two monolayers. From the experimental value $d_{HH} \simeq 3.53$ nm (8) and our simulation result $d_{HH} \simeq 3.64\, r_0$, we obtain the physical length scale $r_0 \simeq 1.0$ nm. From a comparison of the experimentally measured lateral diffusion coefficient $D \simeq 5\, \mu m^2/s$ of DMPC (9) to our simulation result $D \simeq 5.7 \cdot 10^{-4} r_0^2 / t_0$, we obtain the physical time scale $t_0 \simeq 0.114$ ns.

Simulations with Confining Potentials. In our simulations with confining membrane potentials, we impose additional harmonic potentials

$$V_{conf}(z) = \frac{1}{2} k_{conf}(z - z_0)^2 \qquad \textbf{[S10]}$$

on one of the three head beads of each lipid in the two distal monolayers of the apposing membranes—that is, in the two monolayers that do not face the other membrane. The potential is imposed on the head bead that is connected to the left side chain of the lipid molecule shown in Fig. 1A. The z-direction of our simulation box is on average perpendicular to the membranes. The three red data points in Fig. 4 are from simulations with the rather weak confining strengths $k_{conf} = 1, 2$ and $4\, k_B T/\text{nm}^2$ (from

right to left). The membrane tensions in these simulations are 0.13 ± 0.02, -0.15 ± 0.03, and $-0.49 \pm 0.01\, k_B T/\text{nm}^2$ for the confining strengths 1, 2, and $4\, k_B T/\text{nm}^2$, respectively.

Analysis of Binding Kinetics

Maximum-Likelihood Estimation of Rate Constants. We complement here the analysis of the binding kinetics described in the main text by (i) a derivation of the time-dependent probability $P_n(t)$ of a state with n receptor–ligand bonds and (ii) an estimation of the errors for the rate constants obtained by this analysis.

In Fig. S2A, the number of bonds n is displayed as a function of time for a short segment of a simulation trajectory of our largest membrane system with 15 receptors and 15 ligands. A central quantity for extracting the binding kinetics from our simulation trajectories is the probability $P_n(t)$ of staying for a dwell time t in state n. For a Markov process, we have

$$P_n(t + \Delta t) = P_n(t)P_n(t + \Delta t | t), \qquad \textbf{[S11]}$$

where $P_n(t + \Delta t | t)$ is the conditional probability of remaining in state n from time t to $t + \Delta t$. For small time windows Δt, this probability is

$$P_n(t + \Delta t | t) = 1 - \left[k_+^{(n)} + k_-^{(n)} \right] \Delta t, \qquad \textbf{[S12]}$$

where $k_+^{(n)}$ is the transition rate from state n to state $n + 1$, and $k_-^{(n)}$ is the transition rate from state n to state $n - 1$. The probabilities of transitions from state n to states $n \pm 2, n \pm 3, \ldots$ are negligible for small Δt. From Eqs. S11 and S12, we obtain

$$\frac{P_n(t + \Delta t) - P_n(t)}{\Delta t} = -P_n(t)\left[k_+^{(n)} + k_-^{(n)} \right], \qquad \textbf{[S13]}$$

which leads to

$$\frac{dP_n(t)}{dt} = -P_n(t)\left[k_+^{(n)} + k_-^{(n)} \right] \qquad \textbf{[S14]}$$

for $\Delta t \to 0$. The solution of Eq. S14 is the exponential dwell-time distribution

$$P_n(t) = e^{-\left[k_+^{(n)} + k_-^{(n)} \right]t}. \qquad \textbf{[S15]}$$

Fig. S2B illustrates that the histogram of dwell times in state $n = 5$ obtained from our DPD simulations with 15 anchored receptors and ligands fits well to an exponential distribution.

The variances $\delta^2 k$ of the maximum likelihood estimators can be estimated by the Cramer–Rao lower bound $\delta^2 k = (-d^2 \ln L / dk^2)^{-1}$ (10). For the likelihood function L given in Eq. 17 and $k = k_{on}^{(n)}$ or $k_{off}^{(n)}$ given in Eq. 18, we obtain as errors of our rate constant estimates

$$\delta k_{on}^{(n)} \simeq \frac{k_{on}^{(n)}}{\sqrt{N_n^+}} \qquad \textbf{[S16]}$$

and

$$\delta k_{off}^{(n)} \simeq \frac{k_{off}^{(n)}}{\sqrt{N_n^-}}. \qquad \textbf{[S17]}$$

Binding of Soluble Receptors and Ligands. In addition to the membrane systems described in the main text, we have determined the binding kinetics of soluble receptor and ligand molecules that lack the transmembrane anchor. We have considered a single soluble receptor and a single soluble ligand randomly placed in water contained in simulation boxes with the four different sizes $L_x = L_y = L_z = 20$ nm, 24 nm, 28 nm, and 32 nm. Within the statistical errors, the 3D on- and off-rate constants

k_{on} and k_{off} and the binding equilibrium constant K_{3D} are independent of the box size (Fig. S3). We obtain the estimates $k_{on} = (6.2 \pm 0.2) \cdot 10^7 \mathrm{nm}^3/\mathrm{s}$, $k_{off} = (4.0 \pm 0.1) \cdot 10^5/\mathrm{s}$, and $K_{3D} = (157 \pm 6) \mathrm{nm}^3$.

Receptors and Ligands with Increased Binding Energy. To illustrate that our general results for the ratio of K_{2D} and K_{3D} do not depend on the values of the on- and off-rate constants or binding constants, we have performed additional simulations in which the binding strength F_m of the receptors and ligands is increased from our standard value $16\,k_BT/r_0$ (Eq. **S8**) to the value $20\,k_BT/r_0$. For the larger binding strength $20\,k_BT/r_0$, we obtain the binding constant $K_{3D} = (537 \pm 23) \mathrm{nm}^3$ and the rate constants $k_{on} = (6.6 \pm 0.2) \cdot 10^7 \mathrm{nm}^3/\mathrm{s}$ and $k_{off} = (1.23 \pm 0.04) \cdot 10^5/\mathrm{s}$ of our soluble receptors and ligands. The increase in the binding strength and binding energy by 25% thus increases the binding constant K_{3D} by a factor 3.4 ± 0.2, mainly due to a decrease in the off-rate k_{off}. From simulations with tensionless membranes of area $14 \times 14\,\mathrm{nm}^2$ at the optimal membrane separation, we obtain the value $K_{2D} = (2820 \pm 60) \mathrm{nm}^2$ for the binding strength $20\,k_BT/r_0$, which is a factor 3.4 ± 0.1 larger than the value $K_{2D} = (829 \pm 12) \mathrm{nm}^2$ for this membrane system from simulations with our standard binding strength $16\,k_BT/r_0$ (see dark blue data point indicated by the left arrow in Fig. 4). The relative membrane roughness $\xi_\perp$ is determined by the membrane area in this system and, thus, independent of the binding strength within numerical accuracy. Because the increase in the binding strength increases both K_{2D} and K_{3D} by the same factor, the ratio K_{2D}/K_{3D} of the binding constants does not change. For the increased binding strength $20\,k_BT/r_0$, the rate constants of the membrane-anchored receptors and ligands are $k_{on} = (7.6 \pm 0.1) \cdot 10^7 \mathrm{nm}^2/\mathrm{s}$ and $k_{off} = (2.69 \pm 0.04) \cdot 10^4/\mathrm{s}$ in this membrane system. For our standard binding strength $16\,k_BT/r_0$, these rate constants are $k_{on} = (7.3 \pm 0.1) \cdot 10^7 \mathrm{nm}^2/\mathrm{s}$ and $k_{off} = (8.8 \pm 0.1) \cdot 10^4/\mathrm{s}$.

Calculation of Binding Free Energies

Binding Free Energy of Soluble Receptors and Ligands. The binding equilibrium constant K_{3D} of a single soluble receptor and a single soluble ligand molecule in a volume V is related to the binding free energy ΔG_{3D} of the molecules via Eq. **2**. The binding free energy can be written as

$$\Delta G_{3D} = -k_BT(\ln Z_b - \ln Z_u), \quad [\text{S18}]$$

where Z_b and Z_u are the configurational integrals in the bound and unbound state of the molecules. For rod-like receptors and ligands, the configurational integral in the unbound state is

$$Z_u \simeq 2\pi V \int_0^\pi \sin\theta \, d\theta = 4\pi V \quad [\text{S19}]$$

in the dilute limit $V \to \infty$, where θ is the angle between the two molecules. The configurational integral in the unbound state is the product of the translational phase space volume V and the rotational phase space volume 4π of the unbound receptor relative to the ligand.

To calculate the configurational integral Z_b in the bound state of the molecules, we follow a standard approach that is based on a harmonic expansion of the potential of mean force $U(r_x, r_y, r_z, \theta)$ between the interaction beads of the two bound molecules around its minimum U_0 (11, 12):

$$U(r_x, r_y, r_z, \theta) \simeq U_0 + \sum_{q=x,y,z} \frac{k_q}{2}(r_q - r_{q,0})^2 + \frac{k'_\theta}{2}\theta^2. \quad [\text{S20}]$$

Here, (r_x, r_y, r_z) is the distance vector between the beads. For definiteness, we assume that the z-direction is parallel to the ligand, and thus, on average parallel to the receptor–ligand complex, which attains its potential minimum for $\theta = 0$—that is, for a collinear orientation of the receptor and ligand. With Eq. **S20**, the configurational integral in the bound state can be approximated as

$$Z_b \simeq e^{-U_0/k_BT} Z_{\text{trans}} Z_{\text{rot}}, \quad [\text{S21}]$$

with the translational integral

$$Z_{\text{trans}} \simeq \prod_{q=x,y,z} \int_{-\infty}^\infty e^{-\frac{1}{2}k_q(r_q - r_{q,0})^2/k_BT} dr_q = (2\pi)^{3/2} \xi_x \xi_y \xi_z \quad [\text{S22}]$$

and the rotational integral

$$Z_{\text{rot}} \simeq 2\pi \int_0^\pi e^{-\frac{1}{2}k'_\theta \theta^2/k_BT} \sin\theta \, d\theta \simeq 2\pi\sigma_b^2 \quad \text{for} \quad k'_\theta \gg k_BT. \quad [\text{S23}]$$

Here, $\xi_q = (k_BT/k_q)^{1/2}$ and $\sigma_b = (k_BT/k'_\theta)^{1/2}$ are the SDs of the Gaussian distributions for the coordinates $q = x, y, z$ of the binding vector and the binding angle θ, which result from the harmonic approximation of the potential of mean force in Eq. **S20**. The integrals Z_{trans} and Z_{rot} involve three translational and two rotational degrees of freedom. Based on these integrals, the binding free energy ΔG_{3D} defined in Eq. **S18** can be written as

$$\Delta G_{3D} \simeq U_0 + \Delta G_{\text{trans}} + \Delta G_{\text{rot}}, \quad [\text{S24}]$$

with the change $\Delta G_{\text{trans}} = -k_BT \ln(Z_{\text{trans}}/V)$ in translational free energy and the change $\Delta G_{\text{rot}} = -k_BT \ln(Z_{\text{rot}}/4\pi)$ in rotational free energy during binding.

We now decompose the translational free-energy change ΔG_{trans} into (*i*) an entropic contribution

$$-T\Delta S_{\text{trans}} = T\frac{\partial \Delta G_{\text{trans}}}{\partial T} = -k_BT \ln\left[\frac{V_b}{V}\right] \quad [\text{S25}]$$

with the bound-state translational phase space volume

$$V_b = e^{3/2} Z_{\text{trans}} = (2\pi e)^{3/2} \xi_x \xi_y \xi_z \quad [\text{S26}]$$

and (*ii*) an enthalpic contribution $\Delta U_{\text{trans}} = \Delta G_{\text{trans}} + T\Delta S_{\text{trans}} = \frac{3}{2}k_BT$. The factor $e^{3/2}$ in Eq. **S26** results from the temperature dependence of the SDs ξ_x, ξ_y, and ξ_z. Similarly, we decompose the rotational free-energy change ΔG_{rot} into (*i*) an entropic contribution

$$-T\Delta S_{\text{rot}} = T\partial\Delta G_{\text{rot}}/\partial T = -k_BT \ln[\omega_b/4\pi] \quad [\text{S27}]$$

with the bound-state rotational phase space volume

$$\omega_b = eZ_{\text{rot}} = 2\pi e\sigma_b^2 \quad [\text{S28}]$$

and (*ii*) an enthalpic contribution $\Delta U_{\text{rot}} = \Delta G_{\text{rot}} + T\Delta S_{\text{rot}} = k_BT$. The binding free energy ΔG_{3D} then can be written as the sum of enthalpic and entropic contributions as in Eq. **3** with the binding enthalpy

$$\Delta U = U_0 + \Delta U_{\text{trans}} + \Delta U_{\text{rot}} = U_0 + \frac{5}{2}k_BT. \quad [\text{S29}]$$

Binding Free Energy of Membrane-Anchored Receptors and Ligands. Analogous to the case of soluble molecules, we now consider a single receptor and a single ligand that are anchored in two apposing membranes of area A. Our aim is to decompose the binding free energy ΔG_{2D}, which is related to the apparent

binding constant K_{2D} of the molecules via Eq. **5**, into the sum of an enthalpic contribution ΔU and entropic contributions. We assume that the binding interface of the membrane-anchored molecules is identical with the binding interface of the soluble counterparts of the molecules, which lack the membrane anchors (13). This assumption is supported by the distributions of binding distances and angles for our soluble and membrane-anchored receptor–ligand complexes (Fig. S4). The binding enthalpy ΔU of the membrane-anchored receptor and ligand molecules is then identical to the binding enthalpy of the soluble molecules.

Because the anchored molecules diffuse along the membranes, the free-energy contribution from the translational entropy change during binding is

$$-T\Delta S_{\text{trans}} \simeq -k_B T \ln\left[\frac{A_b}{A}\right], \qquad \textbf{[S30]}$$

where A_b is the translational area of the bound receptor–ligand complex in analogy to Eq. **S25**. The two membranes are on average perpendicular to the receptor–ligand complex. In analogy to Eq. **S26**, the bound-state translational area of the complex is then:

$$A_b = 2\pi e \xi_x \xi_y, \qquad \textbf{[S31]}$$

where ξ_x and ξ_y are the SDs of the binding vector coordinates in the two directions perpendicular to the complex and parallel to the membranes. In our simulations, the distributions of the binding vector coordinates x and y perpendicular to the complex are identical for the soluble and anchored molecules (Fig. S4A).

In analogy to Eqs. **S27** and **S28**, the free-energy contribution from rotational entropy changes of the anchored molecules can be calculated as

$$-T\Delta S_{\text{rot}} = -k_B T \ln\left[\frac{\omega_b \omega_{\text{RL}}}{\omega_{\text{R}}\omega_{\text{L}}}\right], \qquad \textbf{[S32]}$$

where $\omega_{\text{R}} = 2\pi e \sigma_{\text{R}}^2$ and $\omega_{\text{L}} = 2\pi e \sigma_{\text{L}}^2$ are the rotational phase space volumes of the unbound receptor and unbound ligand relative to the membrane, and $\omega_{\text{RL}} = 2\pi e \sigma_{\text{RL}}^2$ is the rotational phase space volume for the bound receptor or bound ligand relative to the membrane. Here, σ_{R}, σ_{L}, and σ_{RL} are the SDs of the anchoring angle distributions for the unbound and bound receptor and ligand molecules shown in Fig. S5. Eq. **S32** implies that the binding angle distribution is significantly narrower than the anchoring angle distribution of the bound receptors and ligands. The binding angle distribution then is not affected by the anchoring and is practically identical for the soluble and anchored molecules (Fig. S4). Because the rotational degrees of freedom for the binding angle thus are independent from the anchor rotations, the overall rotational phase space volume for the receptor–ligand complex is the product of the volume ω_{RL} for the rotation of the receptor (or ligand) relative to the membrane and the volume ω_b of the ligand (or receptor) relative to its binding partner. Because our receptor

and ligand molecules have identical anchors, the rotational phase space volume ω_{RL} is identical for the ligand or receptor. However, Eq. **S32** should also hold for different anchoring of receptors and ligands if the binding angle distribution is sufficiently narrow. The receptor–ligand complex is then rather stiff, and the anchoring angles for the receptor and ligand are rather similar because the membranes are on average parallel.

In addition to the translational and rotational entropy loss ΔS_{trans} and ΔS_{rot} of the molecules, the binding of anchored receptor and anchored ligand molecules also leads to an entropy loss ΔS_{mem} of the membranes, as the bound receptor–ligand complex constrains the membrane shape fluctuations. Here, we approximate the receptor–ligand complex as a harmonic constraint $(b/2)l_i^2$ of the local membrane separation l_i with strength b. For such a harmonic constraint, the purely entropic free-energy change of the membrane has been calculated exactly as (14)

$$-T\Delta S_{\text{mem}} = \frac{k_B T}{2}\ln\left[1 + \frac{b\xi_\perp^2}{kT}\right] = \frac{k_B T}{2}\ln\left[1 + \frac{\xi_\perp^2}{\xi_{\text{RL}}^2}\right], \qquad \textbf{[S33]}$$

where $\xi_{\text{RL}} = \sqrt{kT/b}$ is the SD for fluctuations of the local separation l_i within the harmonic constraint. With Eqs. **S30**, **S32**, and **S33**, we obtain the decomposition of the binding free energy ΔG_{2D} of the anchored receptors and ligands given in Eq. **6**.

Results for Our Model. In our harmonic approximation, the changes in rotational and translational entropy during binding of receptors and ligands depend on the SDs of the binding vector coordinates, binding angles, and anchoring angles. For our receptors and ligands, these SDs can be calculated from the distributions shown in Figs. S4 and S5. For the soluble receptors and ligands, we obtain the SDs $\xi_x = \xi_y \simeq 0.52$ nm for the binding vector coordinates r_x and r_y in the two directions perpendicular to the receptor–ligand complex from Fig. S4A and the SD $\xi_z \simeq 0.19$ nm for the coordinate r_z parallel to the complex from Fig. S4B. These SDs lead to the estimate $V_b \simeq 3.6$ nm^3 for the translational phase space volume of the bound receptor relative to the ligand (Eq. **S26**). From the binding angle distribution shown in Fig. S4C, we obtain the SD $\sigma_b \simeq 0.084$, which leads to the estimate $\omega_b \simeq 0.12$ for the rotational phase space volume of the bound receptor relative to the ligand.

The distributions of the binding vector coordinates r_x and r_y and the binding angle θ are practically identical for the soluble and anchored receptors and ligands. From the values $\xi_x = \xi_y \simeq 0.52$ nm for the SDs of r_x and r_y, we obtain the estimate $A_b \simeq 4.6$ nm^2 for the translational phase space area of the anchored receptor–ligand complex (Eq. **S31**) and the estimate $\xi_b = V_b/A_b \simeq 0.78$ nm. From the SDs $\sigma_{\text{R}} = \sigma_{\text{L}} \simeq 0.21$ and $\sigma_{\text{RL}} \simeq 0.14$ of the anchoring angle distributions for the unbound and bound receptor and ligand molecules shown in Fig. S5, we obtain the estimates $\omega_{\text{R}} = \omega_{\text{L}} \simeq 0.75$ and $\omega_{\text{RL}} \simeq 0.33$ for the rotational phase space volumes of the molecules.

1. Hoogerbrugge PJ, Koelman JMVA (1992) Simulating microscopic hydrodynamic phenomena with dissipative particle dynamics. *Europhys Lett* 19(3):155–160.
2. Espanol P, Warren P (1995) Statistical mechanics of dissipative particle dynamics. *Europhys Lett* 30(4):191–196.
3. Groot RD, Warren PB (1997) Dissipative particle dynamics: Bridging the gap between atomistic and mesoscopic simulation. *J Chem Phys* 107(11):4423–4435.
4. Goetz R, Lipowsky R (1998) Computer simulations of bilayer membranes: Self-assembly and interfacial tension. *J Chem Phys* 108(17):7397–7409.
5. Shillcock JC, Lipowsky R (2002) Equilibrium structure and lateral stress distribution of amphiphilic bilayers from dissipative particle dynamics simulations. *J Chem Phys* 117(10):5048–5061.
6. Grafmüller A, Shillcock J, Lipowsky R (2007) Pathway of membrane fusion with two tension-dependent energy barriers. *Phys Rev Lett* 98(21):218101.
7. Grafmüller A, Shillcock J, Lipowsky R (2009) The fusion of membranes and vesicles: Pathway and energy barriers from dissipative particle dynamics. *Biophys J* 96(7):2658–2675.

8. Kucerka N, et al. (2005) Structure of fully hydrated fluid phase DMPC and DLPC lipid bilayers using X-ray scattering from oriented multilamellar arrays and from unilamellar vesicles. *Biophys J* 88(4):2626–2637.
9. Orädd G, Lindblom G, Westerman PW (2002) Lateral diffusion of cholesterol and dimyristoylphosphatidylcholine in a lipid bilayer measured by pulsed field gradient NMR spectroscopy. *Biophys J* 83(5):2702–2704.
10. Kay SM (1993) *Fundamentals of Statistical Signal Processing, Volume I: Estimation Theory* (Prentice Hall, Englewood Cliffs, NJ).
11. Luo H, Sharp K (2002) On the calculation of absolute macromolecular binding free energies. *Proc Natl Acad Sci USA* 99(16):10399–10404.
12. Woo H-J, Roux B (2005) Calculation of absolute protein-ligand binding free energy from computer simulations. *Proc Natl Acad Sci USA* 102(19):6825–6830.
13. Wu Y, Vendome J, Shapiro L, Ben-Shaul A, Honig B (2011) Transforming binding affinities from three dimensions to two with application to cadherin clustering. *Nature* 475(7357):510–513.
14. Netz RR (1997) Inclusions in fluctuating membranes: Exact results. *J Phys I* 7(7):833–852.
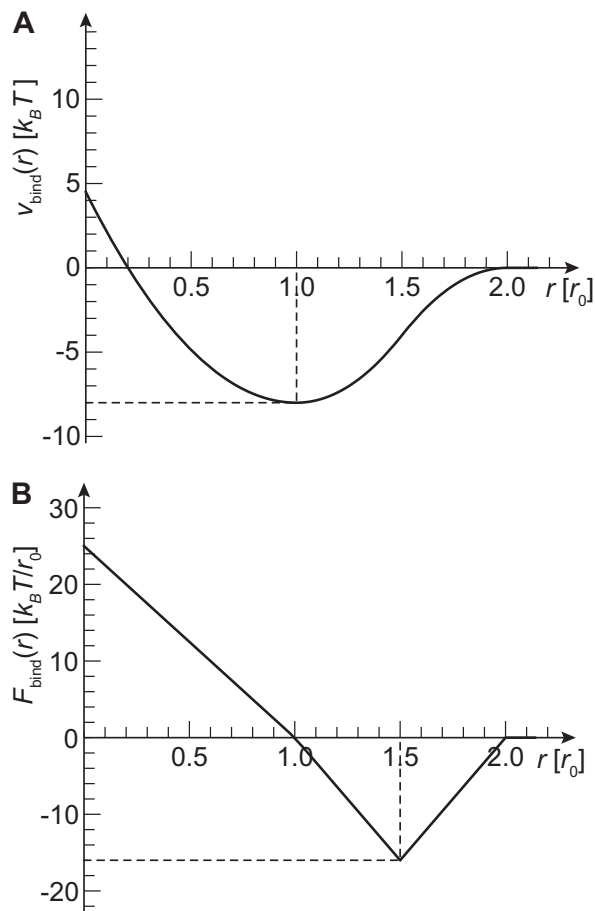
Fig. S1. (*A*) The distance-dependent term $v_{bind}(r)$ of the binding potential between the interaction beads of receptor and ligand molecules (Eq. **S8**). The minimum of the binding potential is $-8\ k_B T$. (*B*) The radial force component corresponding to $v_{bind}(r)$ (Eq. **S9**).
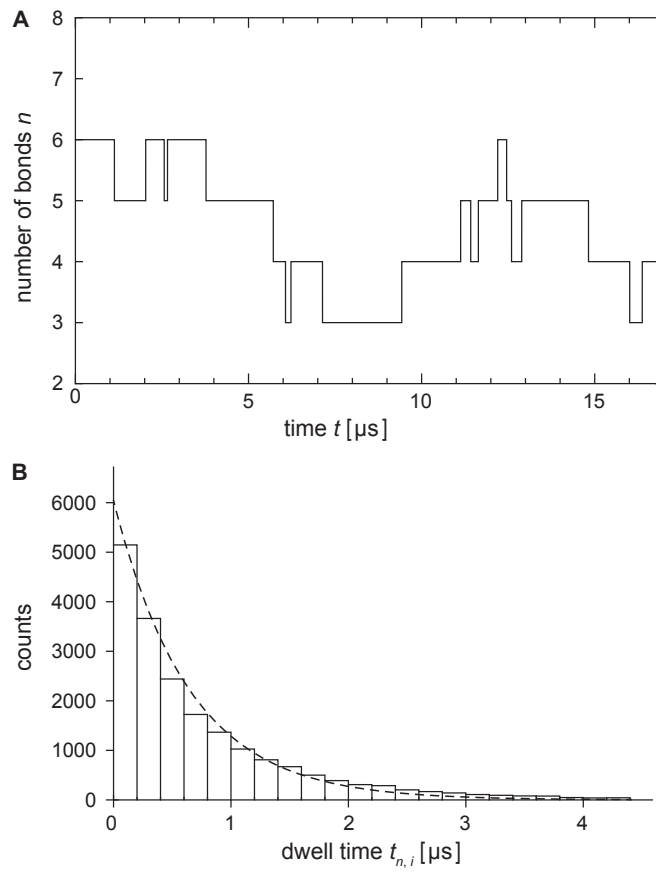
Fig. S2. (*A*) Number of receptor–ligand bonds *n* as a function of time *t* for a short time interval of a simulation with 15 anchored receptors and 15 ligands. (*B*) Dwell-time probabilities in state *n* = 5 obtained from our simulations with 15 anchored receptors and ligands. The dashed line results from an exponential fit.
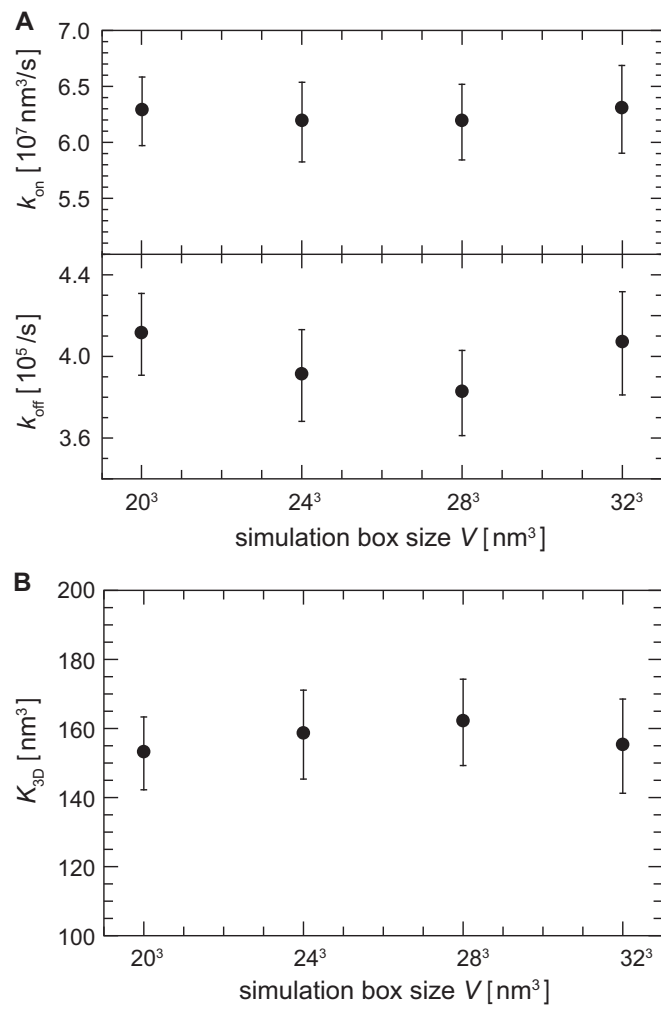
Fig. S3. (*A*) 3D on- and off-rate constants k_{on} and k_{off} and (*B*) binding equilibrium constant $K_{3D} = k_{on}/k_{off}$ obtained from DPD simulations with a single soluble receptor and a single soluble ligand in cubic simulation boxes of different volume V.
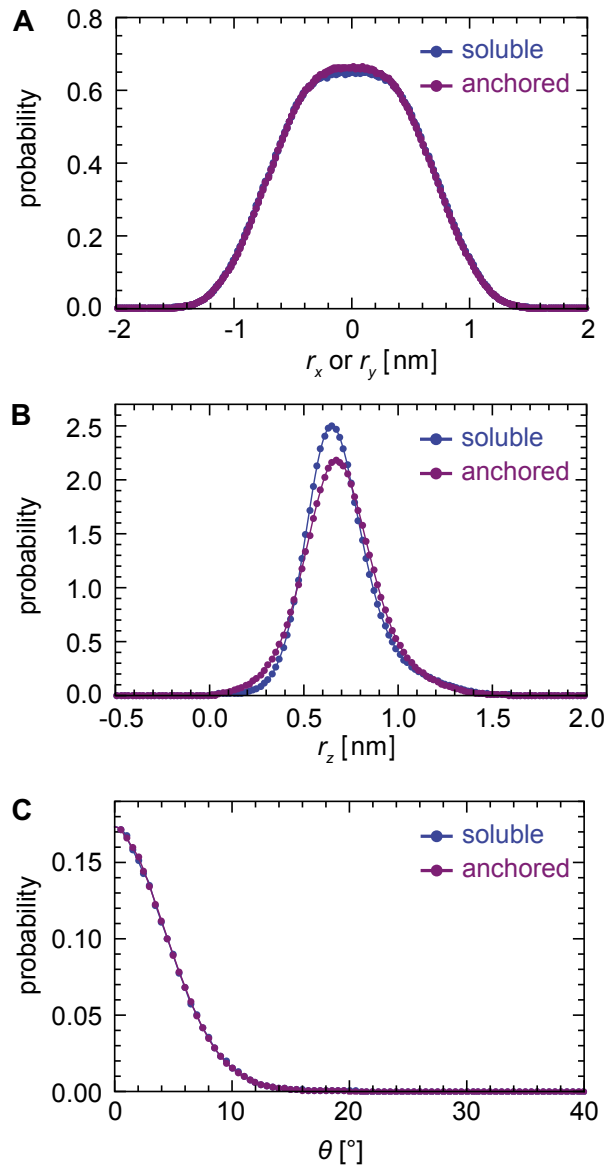
Fig. S4. (*A*) Probability distributions of the binding vector coordinates r_x and r_y in the two directions perpendicular to the receptor–ligand complex of our soluble and anchored molecules. (*B*) Distributions of the binding vector coordinate r_z in the direction parallel to the complex. (*C*) Distributions of the binding angle θ of our soluble and anchored receptor–ligand complexes.
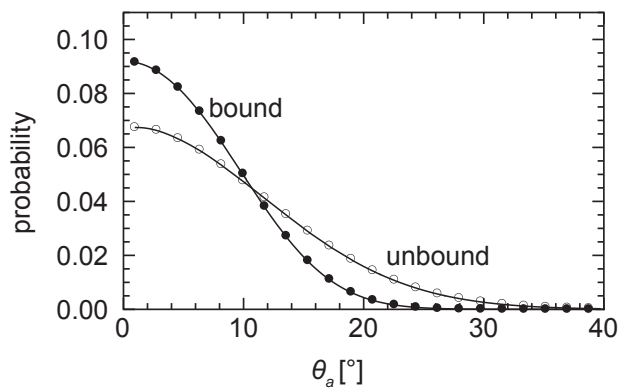

Fig. S5. Probability distributions of the anchoring angle θ_a between the unbound and bound receptors and ligands and the membrane normal.

Table S1. DPD repulsion strength a_{ij} in units of $k_B T / r_0$

Bead type	W	H	C	T_H	T_C	I
W	25	30	75	30	75	25
H	30	30	35	30	35	30
C	75	35	10	35	10	35
T_H	30	30	35	25(75)	25(75)	25(75)
T_C	75	35	10	25(75)	25(75)	25(75)
I	25	30	35	25(75)	25(75)	25(75)

Numbers in parentheses indicate the repulsion strength between the beads of two different receptors or two different ligands.